

Re and Al<sub>2</sub>O<sub>3</sub> were heated with laser beams from both sides. Acting like planar heat sources, the two 'hot plates' eliminate the axial temperature gradient in the sample between the plates. Temperature variation is less than 3% within roughly 30 μm diameter at 2,500 K. Before the melting experiments, the sample was scanned with a laser beam and heated to about 2,000 K to reduce the pressure gradient and to produce a high-pressure solid-phase assemblage. For stable and smooth temperature control, temperatures were increased by adjusting an aperture placed near the beam exit, stepwise, instead of by adjusting power. Each step corresponds to a 50–100 K increase. A 30-μm spot was homogeneously heated by opening the aperture (increasing the step). At the onset of melting, temperature remains constant or drops slightly with the step increment, and then drastically increases (>400 K) within one step. To ensure the reliability of the melting criteria used in this study, we conducted melting experiments at pressures (16–27 GPa) overlapped by the multi-anvil apparatus and the diamond-anvil cell, using the same starting material, and obtained consistent melting temperatures (Fig. 3). We also used the same melting criteria to determine the melting temperature of MgSiO<sub>3</sub>-perovskite previously studied by other investigators, and our results agree with these recent determinations<sup>13,14</sup> (Fig. 3). The temperature runaway phenomena near the onset of melting observed in simple and complex samples were probably a result of the latent heat of melting, followed by melt migrating away from the heated spot because of the large thermal pressure and, finally, the Re foils would have been heated without sample in between. No chemical reaction between Re and sample was observed in the multi-anvil experiments on a scale of 1 μm. The melting temperatures reported here are the last temperatures before melting sets in. Pressures were measured using a ruby-fluorescence technique after each measurement of melting temperature.

Received 22 June; accepted 12 October 1998.

1. Irifune, T. & Ringwood, A. E. Phase transformations in subducted oceanic crust and buoyancy relationships at depths of 600–800 km in the mantle. *Earth Planet. Sci. Lett.* **117**, 101–110 (1993).
2. Ringwood, A. E. Role of the transition zone and 660 km discontinuity in mantle dynamics. *Phys. Earth Planet. Inter.* **86**, 5–24 (1994).
3. Bertka, C. M. & Fei, Y. Mineralogy of Martian interior up to core-mantle boundary pressures. *J. Geophys. Res.* **102**, 5251–5264 (1997).
4. Irifune, T., Ringwood, A. E. & Hiberson, W. O. Subduction of continental crust and terrigenous and pelagic sediments: an experimental study. *Earth Planet. Sci. Lett.* **126**, 351–368 (1994).
5. Irifune, T., Koizumi, T. & Ando, J. An experimental study of the garnet-perovskite transformation in the system MgSiO<sub>3</sub>-Mg<sub>2</sub>Al<sub>2</sub>Si<sub>2</sub>O<sub>12</sub>. *Phys. Earth Planet. Inter.* **96**, 147–157 (1996).
6. Hirose, K. & Fei, Y. Majorite-perovskite transformation on the join MgSiO<sub>3</sub>-Mg<sub>2</sub>Al<sub>2</sub>Si<sub>2</sub>O<sub>12</sub> and its role in the dynamics at the 660-km discontinuity. *Phys. Earth Planet. Inter.* (submitted).
7. Kesson, S. E., Fitz Gerald, J. D. & Shelley, J. M. Mineralogy and dynamics of a pyrolite lower mantle. *Nature* **393**, 252–255 (1998).
8. Faust, J. & Knittle, E. The stability and equation of state of majoritic garnet synthesised from natural basalt at mantle conditions. *Geophys. Res. Lett.* **23**, 3377–3380 (1996).
9. Kesson, S. E., Fitz Gerald, J. D. & Shelley, J. M. G. Mineral chemistry and density of subducted basaltic crust at lower-mantle pressures. *Nature* **372**, 767–769 (1994).
10. Irifune, T. & Ringwood, A. E. Phase transformation in a harzburgite composition to 26 GPa: implications for dynamical behaviour of the subducting slab. *Earth Planet. Sci. Lett.* **86**, 365–376 (1987).
11. Shen, G., Mao, H. & Hemley, R. J. Laser-heated diamond anvil cell technique: double-sided heating with multimode Nd:YAG laser. *Proc. ISAM '96* 149–152 (1996).
12. Yasuda, A., Fujii, T. & Kurita, K. Melting phase relations of an anhydrous mid-ocean ridge basalt from 3 to 20 GPa: implications for the behavior of subducted oceanic crust in the mantle. *J. Geophys. Res.* **99**, 9401–9414 (1994).
13. Zerr, A. & Boehler, R. Melting of (Mg,Fe)SiO<sub>3</sub>-perovskite to 625 kilobars: indication of a high melting temperature in the lower mantle. *Science* **262**, 553–555 (1993).
14. Shen, G. & Lazor, P. Measurement of melting temperatures of some minerals under lower mantle pressures. *J. Geophys. Res.* **100**, 17699–17713 (1995).
15. Zerr, A., Serghiou, G. & Boehler, R. Melting of CaSiO<sub>3</sub> perovskite to 430 kbar and first in-situ measurements of lower mantle eutectic temperatures. *Geophys. Res. Lett.* **24**, 909–912 (1997).
16. Presnall, D. C. & Gasparik, T. Melting of enstatite (MgSiO<sub>3</sub>) from 10 to 16.5 GPa and the forsterite (Mg<sub>2</sub>SiO<sub>4</sub>)-majorite (MgSiO<sub>3</sub>) eutectic at 16.5 GPa: implications for the origin of the mantle. *J. Geophys. Res.* **95**, 15771–15777 (1990).
17. Zerr, A., Diegeler, A. & Boehler, R. Solidus of Earth's deep mantle. *Science* **281**, 243–246 (1998).
18. Kendall, J. M. & Silver, P. Constraints from seismic anisotropy in the lowermost mantle. *Nature* **381**, 409–412 (1996).
19. Kendall, J. M. & Silver, P. Investigating causes of D' anisotropy. *AGU Monogr.* (in the press).
20. Williams, Q. & Garnero, E. Seismic evidence for partial melt at the base of Earth's mantle. *Science* **273**, 1528–1530 (1996).
21. Revenaugh, J. S. & Meyer, R. Seismic evidence of partial melt within a possibly ubiquitous low velocity layer at the base of the mantle. *Science* **277**, 670–673 (1997).
22. Simon, F. E. & Glatzel, G. Fusion-pressure curve. *Z. Anorg. Chem.* **178**, 309 (1929).
23. Kraut, E. A. & Kennedy, G. C. New melting law at high pressures. *Phys. Rev. Lett.* **16**, 608–609 (1966).
24. Boehler, R. Melting temperature of the Earth's mantle and core: Earth's thermal structure. *Annu. Rev. Earth Planet. Sci.* 15–40 (1996).
25. Mao, H. K., Chen, L. C., Hemley, R. J., Jephcoat, A. P. & Wu, Y. Stability and equation of state of CaSiO<sub>3</sub>-perovskite to 134 GPa. *J. Geophys. Res.* **94**, 17889–17894 (1989).

**Acknowledgements.** We thank W. Minarik, J. Konzett, G. Shen and S. Shieh for discussions. This research was supported by the NSE, the Carnegie Institution of Washington, and Japan Society for the Promotion of Science.

Correspondence and requests for materials should be addressed to Y.F. (e-mail: fei@gl.ciw.edu).

## Migration of plutonium in ground water at the Nevada Test Site

A. B. Kersting\*, D. W. Efurđ†, D. L. Finnegan†, D. J. Rokop†, D. K. Smith\* & J. L. Thompson†

\* Isotope Sciences Division, PO Box 808, L-231, Lawrence Livermore National Laboratory, Livermore, California 94550, USA

† Chemical Science and Technology Division, MS J514, Los Alamos National Laboratory, Los Alamos, New Mexico 87545, USA

Mobile colloids—suspended particles in the submicrometre size range—are known to occur naturally in ground water<sup>1,2</sup> and have the potential to enhance transport of non-soluble contaminants through sorption<sup>3</sup>. The possible implications of this transport mechanism are of particular concern in the context of radionuclide transport. Significant quantities of the element plutonium have been introduced into the environment as a result of nuclear weapons testing and production, and nuclear power-plant accidents. Moreover, many countries anticipate storing nuclear waste underground. It has been argued that plutonium introduced into the subsurface environment is relatively immobile owing to its low solubility in ground water<sup>4</sup> and strong sorption onto rocks<sup>5</sup>. Nonetheless, colloid-facilitated transport of radionuclides has been implicated in field observations<sup>6,7</sup>, but unequivocal evidence of subsurface transport is lacking<sup>3,8,9</sup>. Moreover, colloid filtration models predict transport over a limited distance resulting in a discrepancy between observed and modelled behaviour<sup>3</sup>. Here we report that the radionuclides observed in groundwater samples from aquifers at the Nevada Test Site, where hundreds of underground nuclear tests were conducted, are associated with the colloidal fraction of the ground water. The <sup>240</sup>Pu/<sup>239</sup>Pu isotope ratio of the samples establishes that an underground nuclear test 1.3 km north of the sample site is the origin of the plutonium. We argue that colloidal groundwater migration must have played an important role in transporting the plutonium. Models that either predict limited transport or do not allow for colloid-facilitated transport may thus significantly underestimate the extent of radionuclide migration.

The Nevada Test Site (NTS) was the location of 828 underground nuclear tests conducted by the United States between 1956 and 1992<sup>10</sup> (Fig. 1a). As a result, the NTS contains a large inventory (>10<sup>8</sup> Ci) of radioactive material deposited in the subsurface and thus provides a unique opportunity for studying the transport of radionuclide contaminants. During an underground nuclear test, temperatures exceed 10<sup>6</sup> K locally and ~70 tonnes of rock are vaporized and another 700 tonnes of rock are melted for every kiloton (kt) of explosive yield<sup>11</sup>. Most refractory radionuclide species (for example, actinides (except U), rare earths, and alkaline earths) are incorporated into the melt glass that coalesces at the bottom of the cavity. The volatile species (for example, alkali metals, U, Sb, I, Ru and gases—Ar, Kr, Xe) are more broadly distributed in the cavity and overlying rubble chimney created directly above the cavity<sup>12</sup>.

Samples were collected in the northwestern section of the NTS (Fig. 1a) where thick sequences of ash-flow tuffs and rhyolitic lava flows dominate the geology<sup>13,14</sup>. Hydrological gradients in the study area suggest a southwestward and southward flow of ground water with estimated flow velocities ranging from 1 to 80 m yr<sup>-1</sup> (ref. 13). The ER-20-5 well cluster is located 280 m southwest of the Tybo test site and 1.3 km south of the Benham test site (Fig. 1b). The ER-20-5 wells, no. 1 and no. 3, were screened at a depth of 701–784 m and 1,046–1,183 m, respectively.

Groundwater samples were pumped into 200-l drums on three separate occasions over a 16-month period. Unfiltered groundwater

samples were analysed for tritium ( $^3\text{H}$ ),  $\gamma$ -ray-emitting radionuclides and Pu isotopes. Additional 200-l groundwater samples from well no. 1 were collected on the second and third sampling campaigns and filtered in series using 1,000-nm, 50-nm and  $\sim 7$ -nm (100,000 nominal molecular mass) filter sizes. The particulate material ( $>1,000$  nm), two colloidal fractions (1,000–50 nm, and 50–7 nm) and the ultrafiltrate or dissolved fraction ( $< \sim 7$  nm) were separately analysed for  $^3\text{H}$ ,  $\gamma$ -ray-emitting radionuclides and Pu isotopes<sup>15</sup>.

Surface soil samples were collected in the vicinity of the Benham and Tybo nuclear test sites and their  $^{240}\text{Pu}/^{239}\text{Pu}$  isotope ratios measured. Archived melt glass material collected from the cavity region immediately after the detonation of the Benham and Tybo tests was re-analysed for its  $^{240}\text{Pu}/^{239}\text{Pu}$  isotope composition and compared to data previously obtained during the US nuclear test programme. Aliquots from the melt glass were analysed at Los Alamos National Laboratory as well as Lawrence Livermore National

Laboratory to provide external laboratory comparison. Additional experimental details from this study are given elsewhere<sup>16,17</sup>.

Tritium and low specific activities of cobalt (Co), caesium (Cs), europium (Eu) and Pu radioisotopes were detected in the unfiltered ground water (Fig. 2). The levels of radioactivity measured from ground water collected from well no. 3 are significantly lower (1,000–20 times lower) than those measured in ground water from well no. 1. Eu isotopes were not detected in ground water from well no. 3 but may be present below the level of detection ( $\sim 10^{-3}$  Bq l<sup>-1</sup>). Figure 2c illustrates that the same radionuclides and similar levels of radioactivity were detected in the ground water samples obtained from well no. 1 during the three different sampling periods. Analogous results were obtained for ground water samples from well no. 3 (data not shown).

Filtering removed most of the radionuclides from solution, but had essentially no effect on the  $^3\text{H}$  concentration in the filtrates. We found that  $>99\%$  of the Eu and Pu isotopes,  $\sim 91\%$  of the Co, and

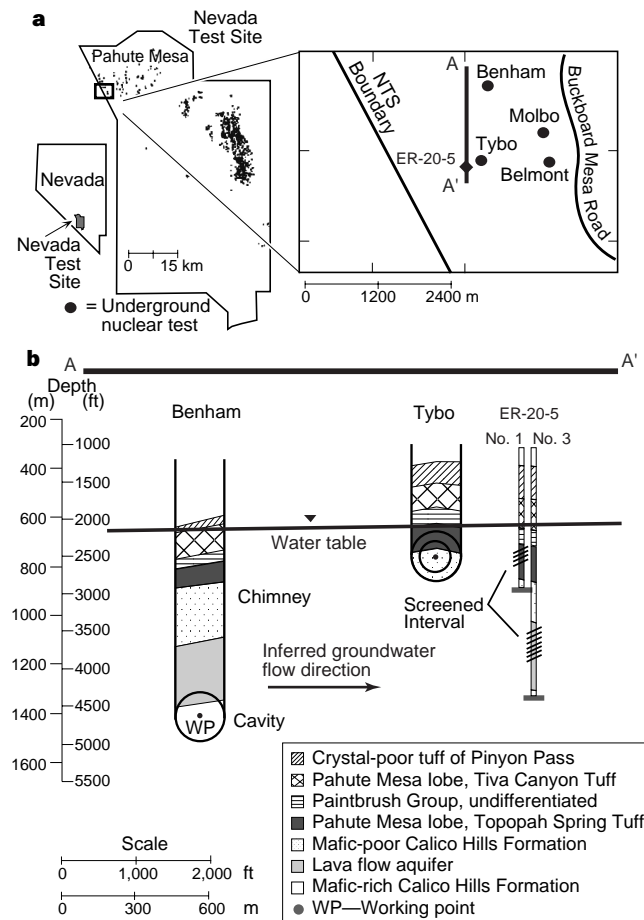


**Figure 1** Location and geology of the study area. **a**, Map of the Nevada Test Site, showing the locations of all detonated underground nuclear tests. An enlarged map of the field area in Pahute Mesa is also shown, giving the location of the well cluster ER-20-5 and all other nearby underground nuclear tests. Molbo (1982) and Belmont (1986) have an announced yield between 20 and 150 kt. **b**, A-A' is a north-south cross-section projecting the Benham and Tybo nuclear tests relative to the ER-20-5 well cluster. Well no. 3 is located  $\sim 30$  m south of well no. 1. The Tybo test was detonated in moderately welded tuff on 14 May 1975 at a depth of 765 m and had an announced yield between 200 and 1,000 kt. Benham was detonated in zholitized bedded tuff on 19 December 1968 at a depth of 1,402 m with a nuclear yield of 1,150 kt. The working point (WP) denotes the location of the nuclear device before detonation. The radius of the cavity is a function of the nuclear yield, density of the rock type and depth of burial (distance from ground surface to WP)<sup>31</sup>. Benham has a calculated cavity radius of 98 m, and Tybo between 62 and 105 m based on the unclassified range in yield.

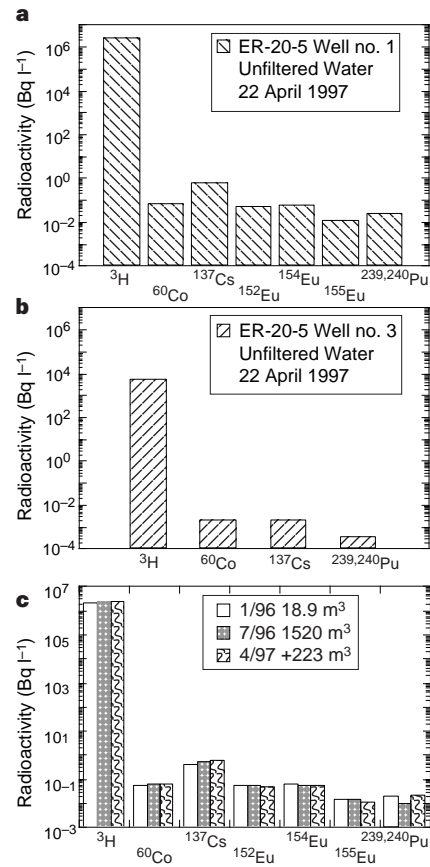


**Figure 2** Comparison of radioactivity detected in unfiltered groundwater samples from ER-20-5 well cluster. Groundwater chemistry of ER-20-5 no. 1 in mg l<sup>-1</sup> is as follows:  $[\text{Cl}^-] = 3.3$ ,  $[\text{SO}_4^{2-}] = 35.0$ ,  $[\text{Na}^+] = 70.0$ ,  $[\text{K}^+] = 3.1$ ,  $[\text{Ca}^{2+}] = 3.2$ ,  $[\text{Mg}^{2+}] = 0.1$ , pH 8.4. For the purposes of comparison, all data were decay-corrected to 22 April 1997, the time of the third sampling. **a**, Concentration of radioactivity measured in unfiltered ground water from the shallower aquifer, pumped from well no. 1. **b**, Concentration of radioactivity measured in unfiltered ground water from the deeper aquifer, pumped from well no. 3. **c**, Comparison of the radioactivity detected in the three groundwater samples collected from well no. 1 over the duration of the field experiment. The first sample was collected after 18.9 m<sup>3</sup> (5,000 gallons) were pumped; the second after  $1.52 \times 10^3$  m<sup>3</sup> (401,000 gallons). The pumps were shut down, and restarted the next spring. An additional  $2.23 \times 10^2$  m<sup>3</sup> (59,000 gallons) of ground water was pumped before the third sample was collected. A total of  $1.76 \times 10^3$  m<sup>3</sup> were pumped from well no. 1 and  $2.19 \times 10^3$  m<sup>3</sup> from well no. 3. Pumping rate is 0.030 m<sup>3</sup> min<sup>-1</sup>.

95% of the Cs in the ground water from well no. 1 were associated with the colloidal and particulate fractions (Fig. 3a).

To determine the source of the radionuclides, and hence the distance they have been transported, we use the  $^{240}\text{Pu}/^{239}\text{Pu}$  isotope ratio to 'fingerprint' the source of the observed Pu in the ground water. Figure 3b shows the normalized  $^{240}\text{Pu}/^{239}\text{Pu}$  isotope ratios measured in this study. The  $^{240}\text{Pu}/^{239}\text{Pu}$  isotope ratio of the unfiltered ground water from well no. 1 matches those of the unfiltered ground water from well no. 3 and the colloidal and particulate fraction from well no. 1. In addition, it uniquely matches the Benham nuclear test and no other. (Each nuclear detonation in the study area is characterized by a unique  $^{240}\text{Pu}/^{239}\text{Pu}$  isotope ratio.) The  $^{240}\text{Pu}/^{239}\text{Pu}$  isotope ratio of the ground water is distinctly different from that of the surface soil samples, eliminating surface contamination as a possible source for the Pu detected in the ground water.

The particulates and two different colloidal size fractions were analysed by X-ray diffraction (XRD) and scanning electron micro-

scopy (SEM). The material was composed of clays (illite and smectite), zeolites (mordenite and clinoptilolite/heulandite), and cristobalite. The same mineral assemblage was detected in all three size fractions ( $>1\ \mu\text{m}$ , 1,000–50 nm, and 50– $\sim 7$  nm). Figure 4 shows SEM images of two distinct morphologies observed; the flat platy minerals and the rod shaped minerals are likely to be clays (illite) and zeolite (mordenite), respectively.

Clays and zeolites are common secondary minerals in altered rhyolitic tuff and smectite, clinoptilolite and mordenite have been specifically identified in the rocks on Pahute mesa<sup>13</sup> and elsewhere in volcanic tuffs at the NTS<sup>18</sup>. Smectite has also been identified as an alteration mineral formed during dissolution of nuclear waste glass<sup>19</sup>. The colloidal minerals identified in ER-20-5 ground water from well no. 1 are consistent with the secondary minerals observed in ground water collected from volcanic tuff aquifers located in the southwestern part of the NTS<sup>20,21</sup>.

Strontium, Cs, Co and actinides (including Pu) have been shown to strongly sorb to clays and zeolites as a result of their large cation-exchange capacity<sup>5,22,23</sup>. For example, Pu sorption experiments involving clinoptilolite with grain sizes between 75 and 500  $\mu\text{m}$  and NTS water with a pH of 7 yielded distribution coefficients of  $K_d > 500\ \text{ml g}^{-1}$  (ref. 5). The zeolite particles and colloids observed in the present study fall within the micrometre and submicrometre size range. Their reduced size will be associated with larger surface areas and is therefore likely to result in higher  $K_d$  values. In fact, recent experiments on the sorption of Pu to montmorillonite suggest that this process may be irreversible on the timescale of the laboratory experiments<sup>24</sup> ( $\sim 1$  year).

The data obtained in this study suggest that Pu and other radionuclides are transported as colloidal material. Although Pu has been shown experimentally to strongly sorb to clays and zeolites, Pu can also exist as an intrinsic colloid, composed of Pu oxide<sup>25</sup>. Both types of colloids have the capacity to be transported by ground water. From this study, we cannot distinguish the colloidal form of the Pu and further study is needed. We suggest that Co, Cs and Eu are sorbed onto the colloidal sized clays and zeolites in the ground water as they do not form intrinsic colloids.

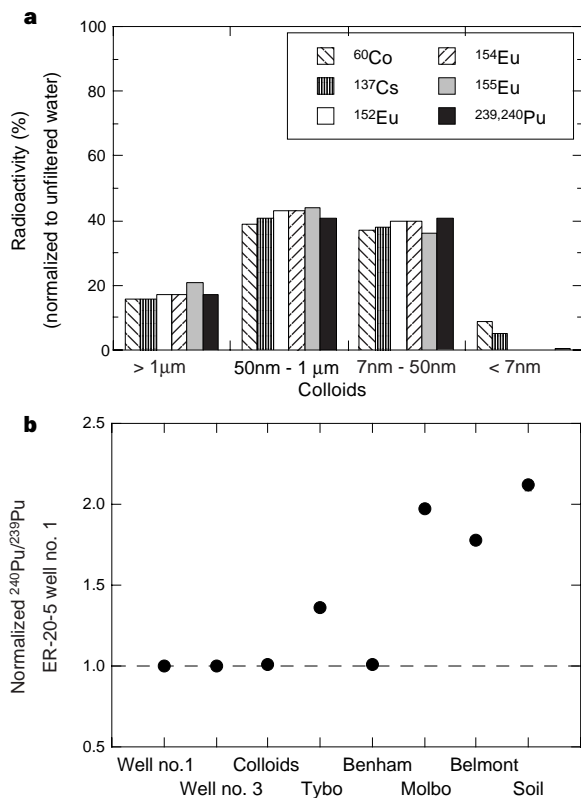


**Figure 3** Radioactivity of the colloidal minerals and comparison of Pu isotope ratios from ER-20-5 ground waters to other nuclear tests. **a**, Comparison of the radioactivity of the colloids collected on the different filter sizes and the ultrafiltrate fraction. Data are normalized to the total radioactivity measured in the unfiltered water. The ultrafiltrate is the water that passed through all the filters ( $< \sim 7$  nm). Filtration occurred in series. A tangential filtration system was used for the 100,000 nominal molecular mass ( $\sim 7$  nm) size filters. **b**, Comparison of the  $^{240}\text{Pu}/^{239}\text{Pu}$  isotope ratios of different samples in this study normalized to the radioactivity measured in ER-20-5 no. 1. Precision is  $\pm 1.5\%$ . The errors plotted are smaller than the symbols used. Results of the Pu isotopic analyses of the archived melt glass material collected from the cavity region immediately after the detonation of Benham and Tybo from both laboratories agree to within 1.5% and also match the original values measured immediately following the nuclear tests. Total laboratory procedural blanks had  $< 2\ \text{pg}$  Pu, significantly below the concentrations analysed and did not contribute to the isotope ratio measured. The concentrations of Pu detected in the soil samples were extremely low ( $< 4\ \text{pg}$  Pu per g sample), and the isotopic ratios distinctly different from the ground water. Values plotted are averages: ER-20-5 no. 1,  $N = 3$ ; ER-20-5 no. 3,  $N = 2$ ; Colloids,  $N = 4$ ; Tybo,  $N = 6$ ; Benham,  $N = 12$ ; Molbo,  $N = 7$ ; Belmont,  $N = 4$ ; and soil,  $N = 2$ . Here  $N$  is the number of samples averaged.

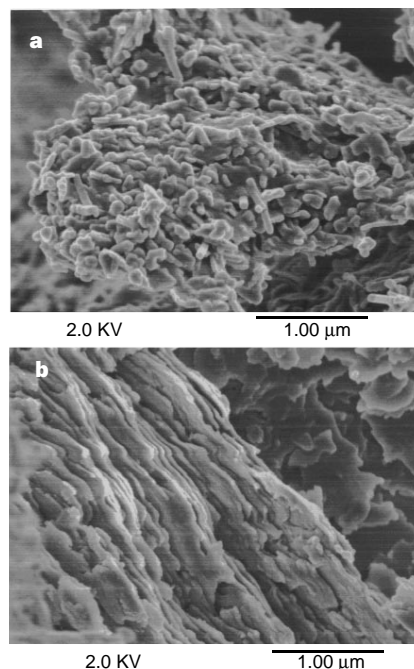


**Figure 4** High-resolution SEM images of the colloids in ER-20-5 no. 1. **a**, The tabular, lath-shaped morphology of the zeolite, mordenite; **b**, the platy appearance of the clay, illite. The two distinct morphologies were observed in all three size fractions ( $> 1\ \mu\text{m}$ , 1,000–50 nm, and 50– $\sim 7$  nm).

The maximum measured concentration of Pu at the ER-20-5 site is  $\sim 10^{-14}$  M. This value is lower than the solubility limits of  $\sim 10^{-8}$  M that have been experimentally determined for the Pu (v) species likely to be present in NTS ground water<sup>4</sup>. The calculated solubility limits ( $10^{-12}$ – $10^{-17}$  M), obtained by assuming that Pu(IV) is in thermodynamic equilibrium<sup>26,27</sup>, bracket the maximum measured Pu concentration. It thus seems that the Pu concentrations in the ground water at ER-20-5 were too low to lead to the precipitation of a solid Pu phase. Our results indicate that <1% of the observed Pu is in the dissolved fraction of the ground water. This finding and the previously reported results of Pu sorption experiments<sup>4,5</sup> are most consistent with Pu migrating as colloidal material and not as a dissolved phase. The concentration of Pu measured is small, and represents only a small fraction of the total Pu associated with the Benham nuclear test.

Based on 40 years of re-drilling underground nuclear test cavities and collecting melt glass samples for test diagnostics, it has been observed that the majority (~98%) of the refractory radionuclides (such as Pu) are incorporated into the melt glass that forms at the bottom of the test cavity<sup>12,28</sup>. In field studies where ground water can be eliminated as a possible transport mechanism, radionuclides were detected at a maximum of a few hundred metres from the original detonation point, and were attributed to gas movement through fractures, or fracture injection of vaporized material at detonation time<sup>29,30</sup>. The possibility that Pu from the Benham test site was blasted and deposited >1.3 km away, in two distinct aquifers separated by 300 m vertically and 30 m horizontally, seems highly unlikely. However, some fraction of the Pu may have been initially injected through fractures a few hundred metres and subsequently transported by ground water.

Molbo, Belmont and Tybo nuclear tests were all detonated after Benham. Although shock waves resulting from underground nuclear blasts can induce radial fractures out to a maximum distance of a few hundred metres (ref. 30), it is unlikely that these detonations blasted material from Benham to ER-20-5, as they were all smaller detonations and by inference shallower. In addition, Pu from these subsequent three tests was not detected in the ground water at ER-20-5.

The high pumping rates ( $0.03 \text{ m}^3 \text{ min}^{-1}$ ) employed may create shear stresses sufficient to generate an increase in the concentration of colloids and thus prevent a quantification of the ambient colloidal load and, by inference, a determination of the minimum or maximum concentration of Pu in the ground water. But the isotope ratio of the Pu measured in ground water from ER-20-5 nevertheless clearly establishes that the radionuclide originates from a specific nuclear event, ~1.3 km to the north. The present work thus demonstrates that Pu is not immobile in the subsurface, but can be transported over significant distances. Pu transport models that only take into account sorption and solubility may therefore underestimate the extent to which this species is able to migrate in ground water. □

Received 24 February; accepted 6 October 1998.

- Degeldre, C. et al. Colloids in water from a subsurface fracture in granitic rock, Grimsel test site, Switzerland. *Geochim. Cosmochim. Acta* **53**, 603–610 (1989).
- McDowell-Boyer, L. M. Chemical mobilization of micron sized particles in saturated porous media under steady flow conditions. *Environ. Sci. Technol.* **26**, 586–593 (1992).
- Ryan, J. N. & Elimelech, M. Colloid mobilization and transport in groundwater. *Colloids Surfaces A: Physicochem. Eng. Aspects* **107**, 1–56 (1996).
- Nitsche, H. et al. Measured Solubilities and Speciations of Neptunium, Plutonium, and Americium in a Typical Groundwater (J-13) from the Yucca Mountain Region Milestone Report 3010-WBS 1.2.3.4.1.3.1 (Rep. LA-12562-MS, Los Alamos National Laboratory, 1993).
- Triay, I. R. et al. Radionuclide Sorption in Yucca Mountain Tuffs with J-13 Well Water: Neptunium, Uranium, and Plutonium (Rep. LA-12956-MS, Los Alamos National Laboratory, 1996).
- Buddemeier, R. W. & Hunt, J. R. Transport of colloidal contaminants in groundwater: radionuclide migration at the Nevada Test Site. *Appl. Geochem.* **3**, 535–548 (1988).
- Penrose, W. R., Polzer, W. L., Essington, E. H., Nelson, D. M. & Orlandini, K. A. Mobility of plutonium and americium through a shallow aquifer in a semiarid region. *Environ. Sci. Technol.* **24**, 228–234 (1990).
- McCarthy, J. F. & Degeldre, C. in *Environmental Particles 2* (eds Buffle, J. & van Leeuwen, H. P.) 247–315 (Lewis, Ann Arbor, 1993).
- Marty, R. C., Bennett, D. & Thullen, P. Mechanism of plutonium transport in a shallow aquifer in

- Mortadad canyon, Los Alamos National Laboratory, New Mexico. *Environ. Sci. Technol.* **31**, 2020–2027 (1997).
- United States Nuclear Tests—July 1945–September 1992 (DOE/NV-209 (Rev. 14), US Department of Energy/Nevada Field Office, 1994).
- Smith, D. K. Characterization of nuclear explosive melt debris. *Radiochim. Acta* **69**, 157–167 (1995).
- Borg, I. Y., Stone, R., Levy, H. B. & Ramspott, L. D. *Information Pertinent to the Migration of Radionuclides in Ground Water at the Nevada Test Site* (Rep. UCRL-52078, Lawrence Livermore National Laboratory, 1976).
- Blankenagel, R. K. & Weir, J. E. J. *Geohydrology of the eastern part of Pahute Mesa, Nevada Test Site, Nye County, Nevada Geol. Surv. Prof. Pap. 712-B* (1973).
- Lacznik, R. J., Cole, J. C., Sawyer, D. A. & Trudeau, D. A. *Summary of Hydrogeologic Controls on Ground-Water Flow at the Nevada Test Site, Nye County, NV* (Rep. 96-4109, US Geological Survey, 1996).
- Perrin, R. E., Knobloch, G. W., Armijo, V. M. & Efurud, D. W. Isotopic analysis of nanogram quantities of plutonium by using a SID ionization source. *Int. J. Mass Spectrom. Ion Phys.* **64**, 17–24 (1985).
- Thompson, J. L. *Laboratory and Field Studies Related to radionuclide Migration at the Nevada Test Site October 1, 1996–September 30, 1997* (Rep. LA-13419-PR Ed., Los Alamos National Laboratory, 1998).
- Smith, D. K. et al. *Hydrologic Resources Management Program and Underground Test Area Operable Unit FY 1997 Progress Report* (Rep. UCRL-ID-130792 Ed., Lawrence Livermore National Laboratory, 1998).
- Broxton, D. E., Bish, D. L. & Warren, R. G. Distribution and chemistry of diagenetic minerals at Yucca Mountain, Nye County, Nevada. *Clays Clay Miner.* **35**, 89–110 (1987).
- Bates, J. K., Bradley, J. P., Teetsov, A., Bradley, C. R. & Buchholz ten Brink, M. Colloid formation during waste form reaction: implications for nuclear waste disposal. *Science* **256**, 649–651 (1992).
- Viani, B. E. & Martin, S. I. *Groundwater Colloid Characterization* (UCRL–Lawrence Livermore National Laboratory, 1996).
- Kingston, W. L. & Whitbeck, M. *Characterization of Colloids Found in Various Groundwater Environments in Central and Southern Nevada* (Rep. DOE-NV/10384-36, Desert Research Inst., Las Vegas, 1991).
- Comans, R. N. J. & Hockley, D. E. Kinetics of cesium sorption on illite. *Geochim. Cosmochim. Acta* **56**, 1157–1164 (1992).
- Torstenfeld, B., Rundberg, R. S. & Mitchell, A. J. Actinide sorption on granites and minerals as a function of pH and colloids/pseudocolloids. *Radiochim. Acta* **44/45**, 111–117 (1988).
- Triay, I. R., Lu, N., Cotter, C. R. & Kitten, H. D. *Iron Oxide Colloid Facilitated Plutonium Transport in Groundwater* (Am. Chemical Soc., Las Vegas, 1997).
- Silva, R. J. & Nitsche, H. Actinide environmental chemistry. *Radiochim. Acta* **70/71**, 377–396 (1995).
- Stout, R. B. & Leider, H. *Preliminary Waste Form Characteristics Report Version 1.0* (Rep. UCRL-ID-108314 Rev. 1, Lawrence Livermore National Laboratory, 1994).
- Guillaumont, R. & Adloff, J. P. Behavior of environmental plutonium at very low concentrations. *Radiochim. Acta* **58/59**, 53–60 (1992).
- Levy, H. B. *On Evaluating the Hazards of Groundwater Contamination by Radioactivity from an Underground Nuclear Explosion* (Rep. UCRL-51278, Lawrence Livermore National Laboratory, 1972).
- Nimz, G. J. & Thompson, J. L. *Underground Radionuclide Migration at the Nevada Test Site* (Rep. DOE/NV-346, US Department of Energy, Nevada Field Office, 1992).
- Smith, D. K., Nagle, R. J. & Kenneally, J. M. Transport of gaseous fission products adjacent to an underground nuclear test cavity. *Radiochim. Acta* **73**, 177–183 (1996).
- Hudson, B. C., Jones, E. M., Keller, C. E. & Smith, C. W. *Cavity Radius Uncertainties* (Rep. LA-9211-C, Los Alamos National Laboratory, Monterey, 1981).

**Acknowledgements.** We thank B. A. Martinez, F. R. Roensch, J. W. Chamberlin and G. P. Russ for help with sample analysis, and I. R. Triay, B. E. Viani, R. W. Loughheed, H. F. Shaw, F. J. Ryerson, J. F. Wild and G. B. Hudson for discussions. This work was funded partly by the Underground Test Area Project sponsored by US Department of Energy, Nevada Operations Office. Work was performed under the auspices of the US Department of Energy by Los Alamos National Laboratory and Lawrence Livermore National Laboratory.

Correspondence and requests for materials should be addressed to A.B.K. (e-mail: Kersting@llnl.gov).

## Patterns of recruitment and abundance of corals along the Great Barrier Reef

T. P. Hughes, A. H. Baird, E. A. Dinsdale, N. A. Moltschanivskyj\*, M. S. Pratchett, J. E. Tanner & B. L. Willis

Department of Marine Biology, James Cook University, Townsville, Queensland 4811, Australia

Different physical and biological processes prevail at different scales<sup>1–4</sup>. As a consequence, small-scale experiments or local observations provide limited insights into regional or global phenomena<sup>5–8</sup>. One solution is to incorporate spatial scale explicitly into the experimental and sampling design of field studies, to provide a broader, landscape view of ecology<sup>1–8</sup>. Here we examine spatial patterns in corals on the Great Barrier Reef, across a spectrum of scales ranging from metres to more than 1,700 km. Our study is unusual because we explore large-scale patterns of a

\* Present address: Department of Aquaculture, University of Tasmania, Launceston, Tasmania 7250, Australia.